Electronic Supplementary Material (ESI) for Journal of Materials Chemistry A.

16.55% Efficiency Ternary Organic Solar Cells Enabled by Incorporating a Small Molecular Donor

Tingting Yan, Jinfeng Ge, Tao Lei, Wenxia Zhang, Wei Song, Billy Fanady, Danli Zhang, Sanhui Chen, Ruixiang Peng, and Ziyi Ge**

T. T. Yan, J. F. Ge, T. Lei, W. X. Zhang, W. Song, B. Fanady, D. L. Zhang, S. H. Chen, R. X. Peng, Prof. Z. Y. Ge
Ningbo Institute of Materials Technology and Engineering
Chinese Academy of Sciences
Ningbo 315201, P. R. China
E-mail: pengrx@nimte.ac.cn, geziyi@nimte.ac.cn
T. T. Yan, T. Lei, W. X. Zhang, W. Song, Prof. Z. Y. Ge
Center of Materials Science and Optoelectronics Engineering
University of Chinese Academy of Sciences
Beijing 100049, P. R. China

Experimental Section

Materials. PM6, Y6, SM1, PDINO were purchased from Solarmer Materials Inc., PEDOT:PSS (Clevios P VP 4083) was obtained from J&K Chemicals Inc. 1-chloronaphthalene (CN), Chloroform (CF) and other drying solvent were bought from Aldrich Inc. The indium-doped tin oxide (ITO)-coated glass (1.1 mm thick, ≤15 Ω/square) were purchased from Wuhu Token Sciences Co., Ltd. PET flexible substrates were purchased from South China Xiangcheng Technology Co., Ltd.

Characterizations. The UV-vis absorption spectrums test was done in the Spectrophotometer (Perkin-Elmer Lambda 950). Photoluminescence spectroscopy was accomplished on a fluorescence spectrometer (FL3-111, Horiba). The current-voltage (*J-V*) under AM 1.5 G irradiation and electrical conductivity test in the dark were done in the Keithley 2440 source meter with a solar simulator (Newport-Oriel® Sol3A 450W) device and calibrated by a standard Si solar cell. The external quantum efficiency (EQE) spectrums were conducted by the solar cell QE tester (QE-R, Enli Technology Co., Ltd) which was calibrated with a 75W xenon lamp source standard probe. Veeco Dimension 3100V atomic force microscope was used to do the surface morphology and phase diagram test. XEUSS SAXS/WAXS equipment were employed to complete the grazing-incidence wide-angle X-ray scattering (GIWAXS) analyses.

1. Cyclic voltammetry (CV) test

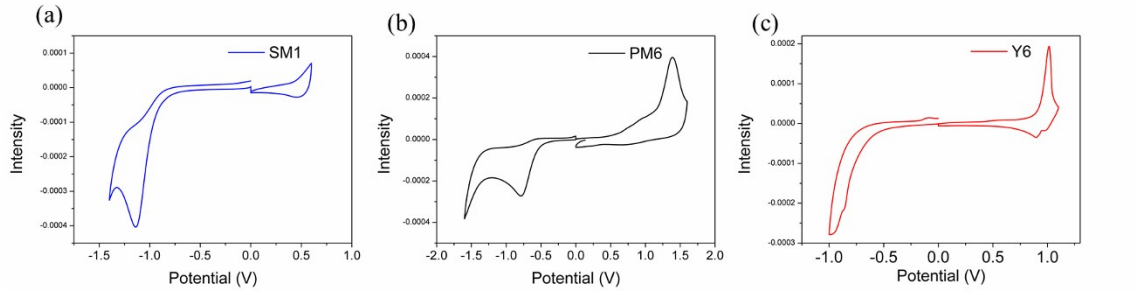

Figure S1. CV test results of (a) SM1 (b) PM6 and (c) Y6, respectively.

Cyclic voltammetry (CV) was used to calculate the energy levels of SM1, PM6 and Y6, Ag/AgCl was used as the reference electrode in anhydrous CH_3CN solution and ferrocene/ferroce-nium (F_c/F_{c+}) was used as internal reference. The following equations were employed to calculate the HOMO and LUMO:

$$HOMO = -[E_{OX} + (4.8 - E_{FC})]\ eV$$

$$LUMO = -[E_{red} + (4.8 - E_{FC})]\ eV$$

Where E_{OX} is the onset of oxidation and the E_{red} relates to the reduction potential, respectively. SM1 exhibits the HOMO and LUMO levels of PM6 are calculated to be -5.25 and -3.33 eV, PM6 exhibits the HOMO and LUMO levels of PM6 are calculated to be -5.50 eV and -3.56 eV, The HOMO and LUMO levels of Y6 are -5.70 and -4.10 eV, respectively.

2. *J-V* and EQE results of optimized ternary devices

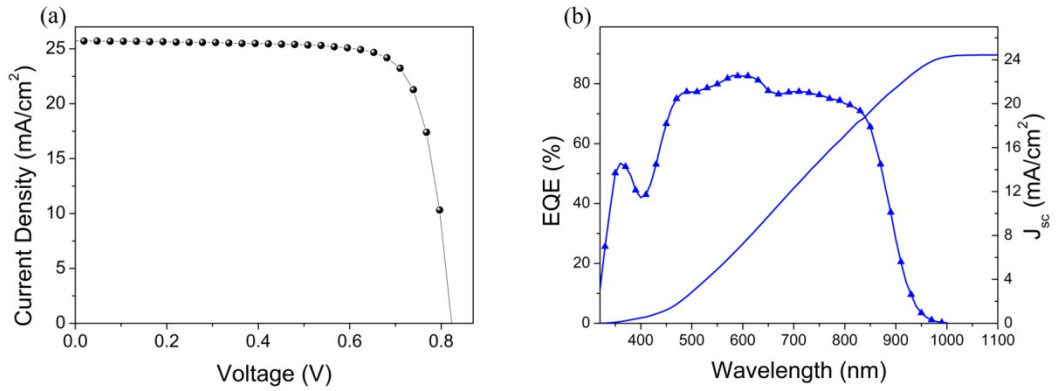

Figure S2. (a) *J-V* curves and (b) EQE spectrum based on PM6:SM1:Y6 ternary devices containing 15 wt% SM1 in donors.

3. Histograms of PCEs

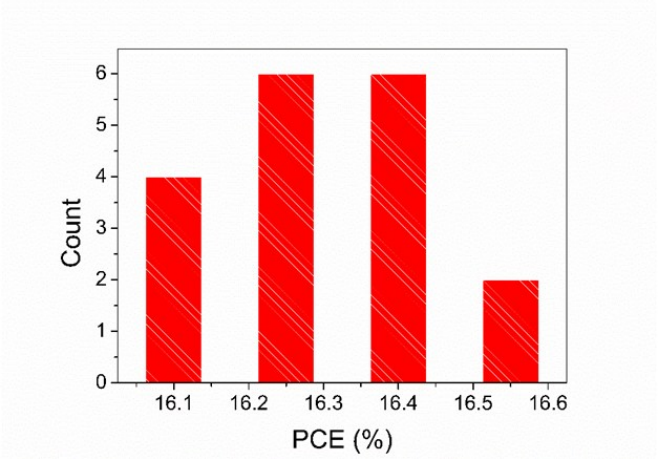

Figure S3. Histograms of PCEs counts for 18 individual devices based on optimal ternary OSCs.

4. Stability of the devices

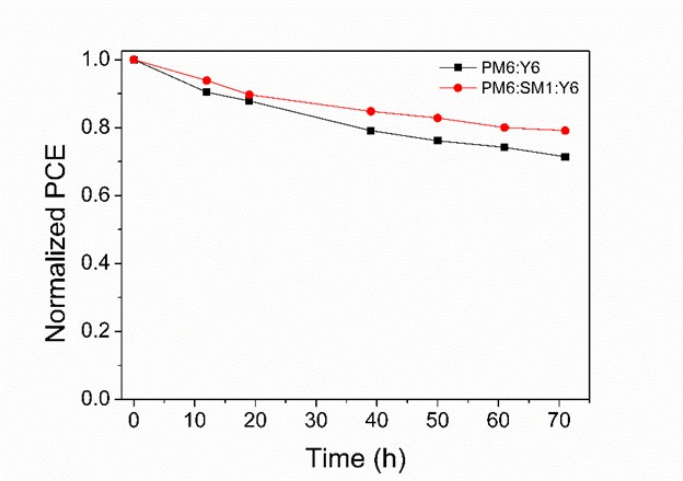

Figure S4. Stability of PM6:Y6 and PM6:SM1:Y6 with 15% SM1 devices tested in the glovebox without encapsulation.

The stability of PM6:Y6 binary and PM6:SM1:Y6 ternary OSCs within 70 h were tested and shown in **Figure S4**. The devices were kept in the glovebox filled with nitrogen and without illumination. The V_{oc} almost kept identical while the FF and J_{sc} decreased to a certain extent in both binary and ternary devices. The PCE in PM6:Y6 binary systems dropped to around 75% of the original value while in PM6:SM1:Y6 ternary systems the PCE still remained over 80% of the original value, indicating that adding the third component small molecular donor may be beneficial for the stability of PM6:Y6 based systems.

5. Hole and electron mobility

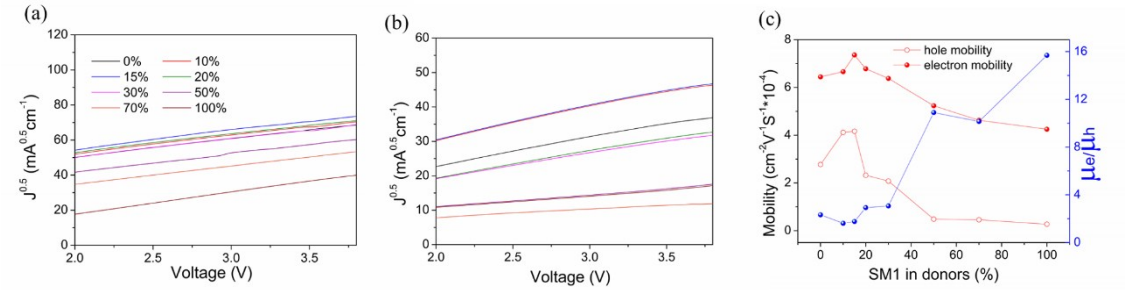

Figure S5. The $J_{0.5}$-V curves of the PM6:SM1:Y6 based ternary devices by adding different ratio of. (a) electron-only devices in a structure of ITO/Al/active layer/PDINO/Al. (b) hole-only devices in a structure of ITO/PEDOT:PSS/active layer/MoO3/Al. (c) electron mobility (μ_e), hole mobility (μ_h) and μ_e/μ_h in ternary blend with different ratio of two donors and acceptor.

The space charge limited current (*SCLC*) method were employed to investigated the carriers mobility of binary and ternary organic solar cells, the structure of the hole-only and electron-only devices were ITO/PEDOT:PSS/active layer/MoO_3/Al and ITO/Al/active layer/PDINO/Al, respectively.

The carrier mobilities (as shown in **Figure S5**) were calculated by fitting the Mott-Gurney square law:

$$J_{SCLC} = \frac{9}{8}\varepsilon_0\varepsilon_r\mu_e\frac{V^2}{L^3}$$

Figure S5a-b shows the $J_{0.5}$-V curves of binary and ternary devices. As shown in **Figure 5c**, the hole and eletron mobilities shows relatively low hole mobility (μ_h) (2.77 × 10^{-4} cm^2 V^{-1} s^{-1}) and electron mobility (μ_e) (6.44× 10^{-4} cm^2 V^{-1} s^{-1}) in the PM6:Y6 binary, the hole and electron mobilities increased as SM1 was addded. After the content of SM1 was above 15%, the mobilities started to decrease and the SM1:Y6 binary systems showed the lowest hole and electron mobilites. The ratios of μ_e/μ_h which refer to the balance of the charge transport and showed lowest value of 1.61 as the content of SM1 was around 15 wt% indicated that the charge transport of hole and eletron were well balanced thus leading to the increase of J_{sc} and FF.

6. Absorption and PL spectrum of SM1 film

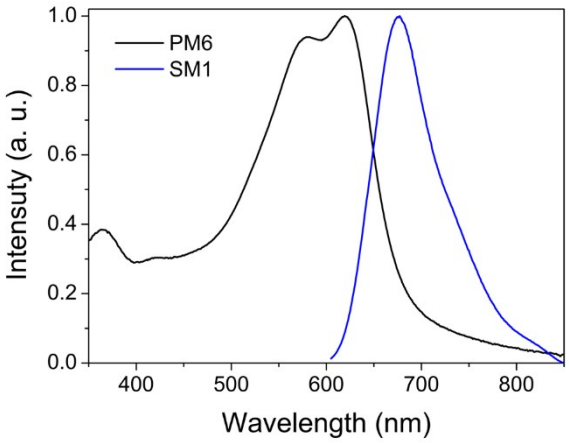

Figure S6. The absorption spectrum of PM6 film and PL spectrum of SM1 film.

7. GIWAXS characterization

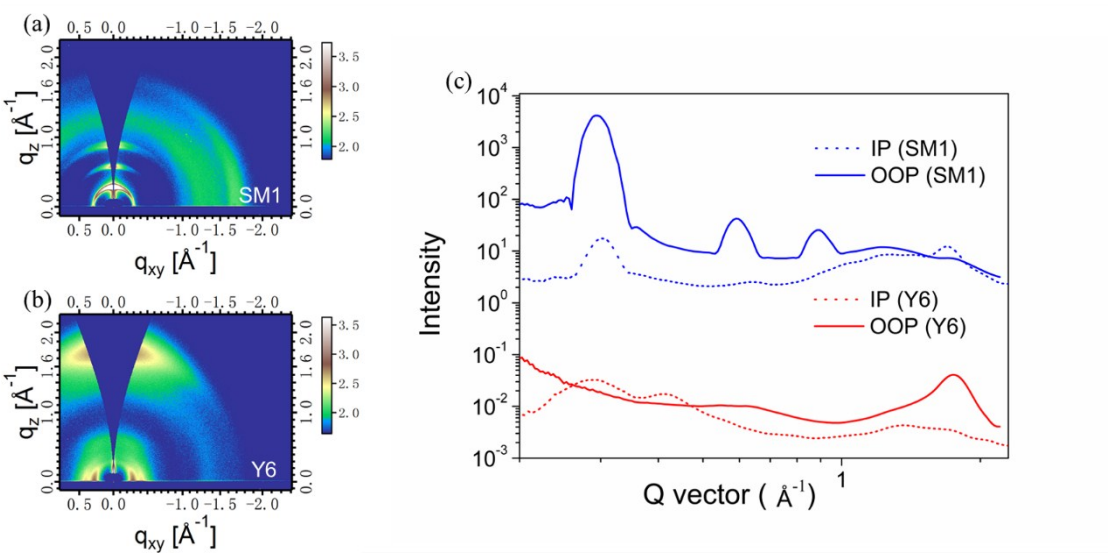

Figure S7. GIWAXS images of (a) SM1 and (b) Y6 neat films, (c) GIWAXS intensity profiles along the in-plane (dotted line) and out-of-plane (solid line) directions for the neat films of PM6 and Y6.

The GIWAXS images of SM1 and Y6 neat films are shown in **Figure S7a-b,** and the GIWAXS intensity profiles along the in-plane (dotted line) and out-of-plane (solid line) directions for the neat films of SM1and Y6 are shown in **Figure S7c**. GIWAXS images and intensity profiles of Y6 were obtained from our previous work (Advanced Materials, 2019, 31, 1902210). There exist (100) peaks along q_z in 0.294 Å^{-1} in the lamellar diffractions and π-π stacking diffractions along q_{xy} in 1.718 Å^{-1} indicating that the SM1 had a preference of edge-on orientation. In addition, Y6 exhibited a strong peak in 0.299 Å^{-1} along the in-plane direction and 1.76 Å^{-1} along the out-of-plane direction, which tends to form face-on orientation.

8. AFM characterization of blend films

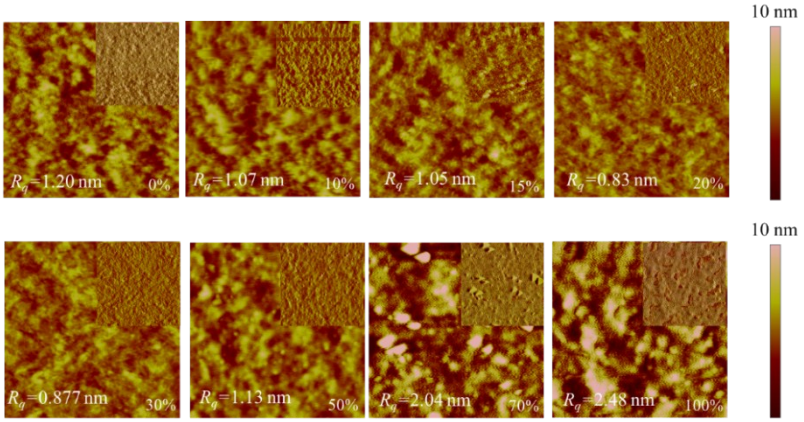

Figure S8. AFM images (2×2μm) of PM6:SM1:Y6 based systems with different blending contents of SM1.